JABET
Journal of Advanced Biotechnology and Experimental Therapeutics

ORIGINAL ARTICLE

J Adv Biotechnol Exp Ther. 2026 Sep; 9(3): 418-430
eISSN: 2616-4760, DOI: 10.5455/jabet.2026.29
Published by www.bsmiab.org

Growth inhibitory action of red *Trapa natans* shell methanolic extract in Ehrlich ascites carcinoma cells by inducing apoptosis through inactivation of NF-kB

Saharia Yeasmin Asha[1], Mst. Ayesha Siddika[2], Mahmud Ismail[1], Arifur Rahman[1], Maksudul Haque[2], Farhadul Islam[1], Syed Rashel Kabir[1], Md. Abdur Rakib[1,*]

[1]Department of Biochemistry and Molecular Biology, University of Rajshahi, Rajshahi-6205, Bangladesh
[2]Department of Biochemistry and Biotechnology, University of Science and Technology Chittagong (USTC), Chattogram-4202, Bangladesh

***Corresponding author**
Md. Abdur Rakib, PhD
Department of Biochemistry and Molecular Biology, University of Rajshahi, Rajshahi-6205, Bangladesh
Email: mar@ru.ac.bd

Academic editor
Md. Abdul Hannan, PhD
Bangladesh Agricultural University, Bangladesh

Article info
Received: 06 April 2026
Accepted: 06 June 2026
Published: 18 June 2026

Keywords
Apoptosis, Carcinoma cells, Molecular docking, NF-kB, *Trapa natans* L.

ABSTRACT

Trapa natans L., commonly known as water chestnut, is a small aquatic herb belonging to the family *Trapaceae*. Its fruit is valued for both nutritional and pharmaceutical properties. This study investigated the anticancer potential of Red *Trapa natans* shell methanolic extract (RTNSME) against Ehrlich ascites carcinoma (EAC) cells. RTNSME demonstrated significant anticancer activity, inhibiting EAC cell growth by 76.05% compared to the untreated cells. DAPI-stained cells revealed nuclear condensation, cell shrinkage, and membrane blebs in RTNSME-treated EAC cells in contrast to untreated cells under Fluorescence microscopy. These findings were supported by RT-PCR analysis of pro-apoptotic and anti-apoptotic genes. RTNSME up-regulated the expression of *p53* and *Bax*, while down-regulating the anti-apoptotic gene *Bcl-2*. Additionally, RTNSME suppressed the activity of the *NF-kB*, further indicating its role in promoting apoptosis. GC-MS analysis of RTNSME identified 35 phytochemical constituents, including some known bioactive and anticancer compounds such as canthaxanthin, dipyridamole, and colchiceinamide. Molecular docking studies suggested that canthaxanthin exhibits the strongest binding affinity and is likely the most potent compound against EAC cells. Overall, this study demonstrates that RTNSME exerts significant anticancer effects on EAC cells, primarily through *NF-kB* inactivation and induction of apoptosis.

INTRODUCTION

Cancer is considered one of the deadliest diseases worldwide, claiming over six million annual deaths [1]. While both synthetic drugs and natural compounds with anticancer properties have shown promise in cancer treatment [2, 3]. Current chemotherapeutic agents are often expensive and associated with severe side effects. Therefore, the development of cost-effective and safer natural therapeutic alternatives is a critical priority in cancer research [4]. Due to their lower toxicity, wide availability, and bioactivity, natural compounds are being explored for their anticancer potential [5].

Trapa natans L., commonly known as water chestnut or water caltrop, is an annual aquatic floating herb belonging to the family *Trapaceae* [6]. It typically grows in lakes, ponds, ditches, and other stagnant water bodies and is widely cultivated in tropical, subtropical, and temperate regions of the world [7]. Two primary varieties of *Trapa natans* are recognized. Various extracts of its fruit have been reported to exhibit a broad spectrum of pharmacological properties, including antimicrobial [8], analgesic [9], anti-inflammatory [10], antidiabetic [11], antioxidant, antiulcer, and antifungal activities [12].

Previous studies have also demonstrated the anticancer potential of *Trapa natans* in several human cancer cell lines, such as human colon cancer (Colo-205), human ductal

Copyright: © by the authors. This article is an open access article distributed under the terms and conditions of the Creative Commons Attribution 4.0 (CC BY 4.0) International license.

breast carcinoma (T47D), and human breast adenocarcinoma (MCF-7) cells [13]. In our earlier study, RTNSME relieved high concentrations of phytochemicals with strong antioxidant activity [14]. However, its anticancer activity against EAC cells has not yet been investigated. Considering these reports, the present study aims to evaluate the anti-proliferative effects of RTNSME on EAC cells and to elucidate its underlying molecular mechanisms. In this study, we report that RTNSME inhibits EAC cell growth by inducing apoptosis through inactivation of *NF-kB*.

MATERIALS AND METHODS

Preparation of red Trapa natans shell methanolic extract (RTNSME)

Mature red *Trapa natans* fruits were procured from a local market in Rajshahi, Bangladesh. The species was taxonomically authenticated by a specialist in the Department of Botany, University of Rajshahi. The red-colored fruits were thoroughly washed with distilled water to remove surface impurities. The shells were manually separated, shade-dried, and then ground into a fine powder using a mechanical grinder. The powdered shell material was stored in an airtight container in a refrigerator until extraction.

The extract was prepared as described by Luqman A. Olayaki *et al.* [15], with slight modifications. Approximately 150 grams of the powdered shell were soaked in 500 mL of methanol (DUKSAN PURE CHEMICALS CO., LTD, Ansan, Korea) and kept under continuous stirring for 24 hours at room temperature. After initial extraction, the mixture was filtered through Whatman No. 1 filter paper, and an additional 100 mL of methanol was added to the residue for re-extraction. The combined filtrates were concentrated using a rotary evaporator (BIOBASE, China) at 37°C to remove the solvent. The resulting dried extract RTNSME), was stored at 4°C in a refrigerator for further use in experiments.

Animals

Swiss albino mice (6 to 8 weeks old, weighing 25 ± 4 g) were obtained from the Department of Pharmacy, Jahangirnagar University, Bangladesh. The animals were housed in standard laboratory conditions with a 12-hour light/dark cycle and maintained at room temperature with proper ventilation. Six mice were kept per cage. All animals were provided with standard laboratory chow and drinking water *ad libitum* throughout the experimental period.

All experimental procedures involving animals were conducted in accordance with ethical guidelines approved by the Institutional Animal, Medical Ethics, Biosafety and Biosecurity Committee (IAMEBBC) for experimentation on Animals, Humans, Microbes, and Living Natural Sources, Institute of Biological Sciences, University of Rajshahi, Bangladesh (Approval No. 117/320 (47)/IAMEBBC/IBSc).

Cell line

Ehrlich ascites carcinoma (EAC) cells were kindly provided by the Department of Pharmacy, Jahangirnagar University, Bangladesh. All procedures involving biosafety and animal handling were conducted in compliance with the guidelines of the Institute of Biological Sciences, University of Rajshahi, Bangladesh. The peritoneal cavity of Swiss albino mice was used for EAC cell culture.

Experimental design

Mice were randomly divided into groups (n=5 per group). This study was divided into four groups. The groups were assigned as follows: Group 1: Untreated control (EAC cell-bearing mice), Group 2: EAC cells treated with 25 mg RTNSME/kg bwt, Group 3: EAC cells treated with 50 mg RTNSME/kg bwt, Group 4: EAC cells treated with 100 mg RTNSME/kg bwt.

Cell growth inhibition determination

Cell growth inhibition was assessed as previously described [16]. On day 0, mice were intraperitoneally inoculated with 1×10^6 EAC cells. After 24 hours, RTNSME was administered at doses of 25, 50, and 100 mg/kg body weight per mouse per day to the respective treatment groups for five consecutive days. A control group received only normal saline. On day 6, all animals were sacrificed, and the ascitic fluid was collected. EAC cells were harvested and counted using a hemocytometer to evaluate the extent of cell growth inhibition.

DAPI staining for morphological appearance and nuclear damage of EAC cells

The induction of apoptosis in EAC cells was assessed as previously described [17]. Both treated and untreated control EAC cells were analyzed using a fluorescence inverted microscope (Olympus IX71, Japan). Initially, the cells were collected and stained with 25 µL of DAPI (Carlroth, Germany) solution (1 mg/mL) at 37°C for 20 minutes. After staining, the cells were washed three times with PBS in the dark to remove excess dye. Morphological changes, including nuclear condensation and fragmentation, were observed under the fluorescence microscope to assess nuclear damage and apoptotic characteristics.

Reverse transcriptase polymerase chain reaction (RT-PCR)

Total RNA was extracted from cells using an RNA extraction kit according to the manufacturer's instructions (FavorPrep, Favorgen, Taiwan). cDNA was synthesized via reverse transcription PCR following the protocol provided with the kit (GoScript™ Reverse Transcription System kit, PROMEGA). The primers used for the experiment are listed in Table 1. The PCR products were subjected to electrophoresis on a 1.0% agarose gel, which was then stained with ethidium bromide. The gel was visualized under a UV transilluminator to assess the amplification of target genes.

Table 1. The sequence of primers used for PCR amplification.

Gene name	Primer sequence references
GAPDH	Forward: (5′-GTGGAAGGACTCATGACCACAG-3′) Reverse: (5′-CTGGTGCTCAGTGTAGCCCAG-3′)
p53	Forward: (5′-CACAAAAACAGGTTAAACCCAG-3′) Reverse: (5′-AGCACATAGGAGGCAGAGAC-3′)
Bcl-2	Forward: (5′-GTGGAGGAGCTCTTCAGGGA-3′) Reverse: (5′-AGGCACCCAGGGTGATGCAA-3′)
Bax	Forward: (5'-GGCCCACCAGCTCTGAGCAGA-3') Reverse: (3'-GCCACGTGGGCGTCCCAAAGT-5')
NF-kB	Forward: (5'-AACAAAATGCCCCACGGTTA-3') Reverse: (3'-GGGACGATGCAATGGACTGT-5')

Measurement of intracellular reactive oxygen species

Intracellular reactive oxygen species (ROS) was assessed as described [18]. Untreated and treated cells were collected from mice peritoneal cavity and washed with PBS. Cells were incubated at 37°C in dark for 30 minutes with 50µM DCFH-DA (Sigma Aldrich, MO, USA). Cells was measured under a fluorescence microscope (Olympus IX71, Japan) at excitation and emission wavelengths of 485 nm and 530 nm, respectively.

Gas chromatography-mass spectrometry analysis

Gas chromatography-mass spectrometry (GC-MS) analysis of RTNSME was performed using a Varian GC spectrophotometer (Model CP-3800, USA) coupled with a Varian Saturn-2200 mass spectrometer. The system was equipped with a flame ionization detector and a VF-5 ms capillary column (30m×0.25 mm, 0.25 µm). The instrument was operated in electron impact mode at 70 eV ionization voltages, with the injector temperature set at 250°C and the detector temperature set at 280°C. A 1µL sample was injected with helium as the carrier gas at a flow rate of 1 mL/min. The column temperature was initially set to 40°C for 1 minute, then ramped to 310°C at a rate of 10°C/min, where it was held for 10 minutes. Chemical compounds were identified and quantified by comparing their mass spectra with the NIST 05 Library database.

Molecular docking simulation

Molecular docking simulations were performed to explore the potential interactions between Bax, Bcl-2, p53, and NF-kB proteins with the compounds Canthaxanthin, Colchiceinamide, and Dipyridamole. The 3D structures of BAX, BCL2, p53, and NF-kB proteins were retrieved from the Protein Data Bank (PDB) (https://www.rcsb.org/) with the following PDB codes: 5W62 (Bax), 2KUA (Bcl-2), 2IOI (p53), and 1MY5 (NF-kB). To eliminate potential interference from water molecules and heteroatoms, these were removed using Biovia Discovery Studio 2021, reducing the possibility of undesired interactions with the receptor proteins. The resulting PDB files were then converted into pdbqt format for docking analysis.

The chemical structures of Canthaxanthin (CID: 5281227), Colchiceinamide (CID: 18397), and Dipyridamole (CID: 3108) were downloaded in 3D SDF format from the PubChem database (https://pubchem.ncbi.nlm.nih.gov/), minimized, and converted into pdbqt format using the PyRx tool. Docking studies were carried out using PyRx with Autodock Vina to predict the binding affinity and interaction between the proteins and compounds. The protein-ligand interactions, including hydrogen bonds, pi-alkyl bonds, hydrophobic interactions, and other relevant bonding types, were analyzed and visualized using BIOVIA Discovery Studio 2021.

Statistical analysis

Experiments were performed in triplicate, and the data are presented as the mean ± standard deviation (SD). Statistical analysis was conducted using one-way analysis of variance (ANOVA), followed by Duncan's multiple range test to compare group means. All analyses were performed using SPSS software (IBM, SPSS version 16). Differences were considered statistically significant at $p< 0.05$.

RESULTS

RTNSME inhibited EAC cell growth

EAC cells were treated with 25, 50, and 100mg/kg bwt RTNSME. RTNSME showed 26.21, 38.15, and 76.05 % of growth inhibition at the doses of 25, 50, and 100mg, respectively, compared to untreated control EAC cells, as shown in Figure 1. As 100mg/kg bwt was found to be significantly more effective against EAC cells. Hence, it was selected to assess all other experiments.

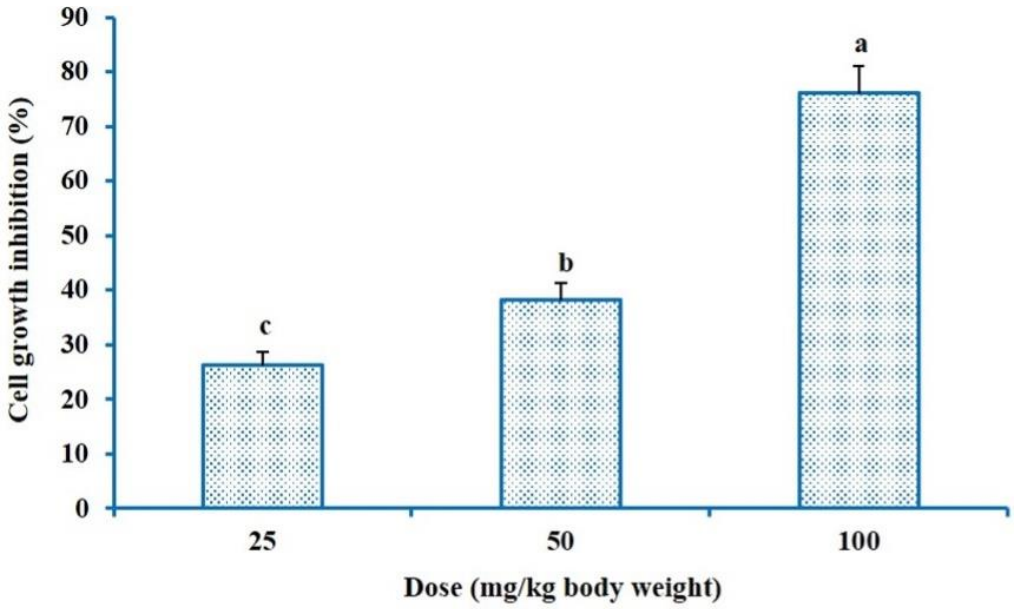


Figure 1. Effects of RTNSME on EAC cell growth inhibition. EAC cells were treated with 25, 50, and 100mg/kg bwt (i.p) of mice. Results are shown as mean ± SD (standard deviation) (n=4). Means with different lowercase letters are significantly different at $p < 0.05$ by Duncan's multiple-range test.

Induction of apoptosis in RTNSME-treated EAC cells

To know the cell death type, DAPI staining was performed on untreated and treated EAC cells. Morphological results showed that EAC cells in the untreated control were found in regular shape with a round nucleus. Conversely, cell membrane shrinkage and nuclear condensation were observed in RTNSME-treated cells. The morphological changes in the 100 mg dose indicate apoptotic EAC cell death as compared to untreated control cells (Figure 2A).

It is known that some apoptotic genes, such as *p53* and *Bax*, and the anti-apoptotic gene *Bcl-2*, play a vital role in apoptotic cell death [19, 20]. Hence, the expression level of pro-apoptotic *p53* and *Bax* and anti-apoptotic *Bcl-2* genes was evaluated by using specific primers. *p53* and *Bax* genes were found up-regulated, and the anti-apoptotic gene, *Bcl-2*, down-regulated in treated cells in comparison with untreated cells. These results indicated mitochondrial dysfunction mediated apoptosis in EAC cells (Figure 2B).

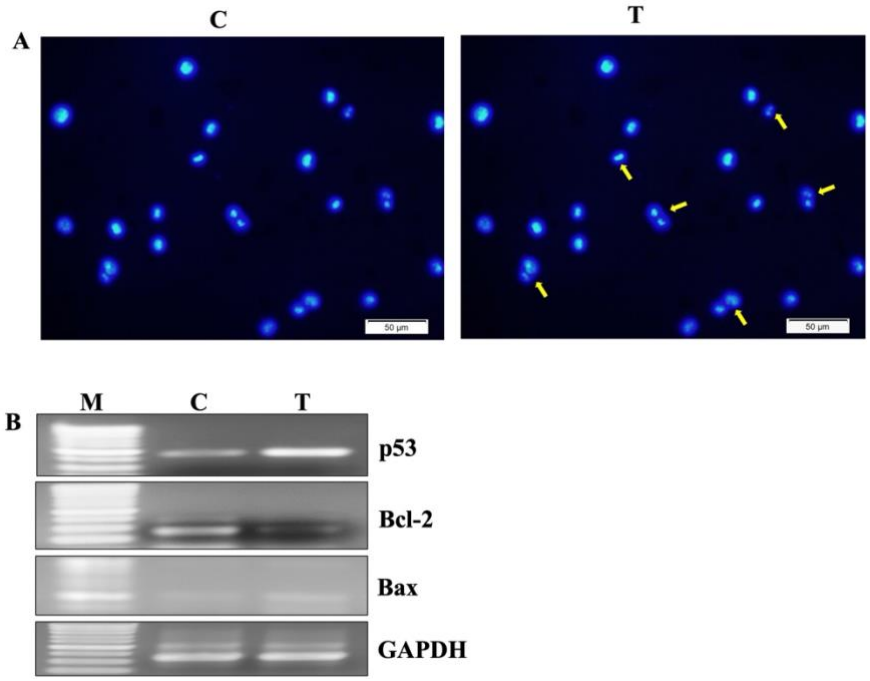


Figure 2. Induction of apoptosis in EAC cells treated with RTNSME. A) DAPI staining of EAC cells treated with RTNSME followed by fluorescence microscopic analysis of cells. B) Expression of *p53*, *Bax*, and *Bcl-2* genes in EAC cells treated with RTNSME. UV-trans illuminator visualizations of *p53*, *Bcl-2*, *Bax*, and *GAPDH*. Here, M: Marker, C: untreated EAC cells, and T: EAC cells treated with RTNSME.

Inactivation of NF-kB by RTNSME in EAC cells

NF-κB regulates cell growth, cell survival, and induces cell apoptosis [21-26]. To understand the association of NF-kB in RTNSME-induced growth inhibition in EAC cells, its expression was evaluated. It was found that RTNSME downregulates *NF-kB* as compared to untreated EAC cells (Figure 3). This result revealed that EAC cell growth inhibition by RTNSME might be due to the inhibition of *NF-kB*.

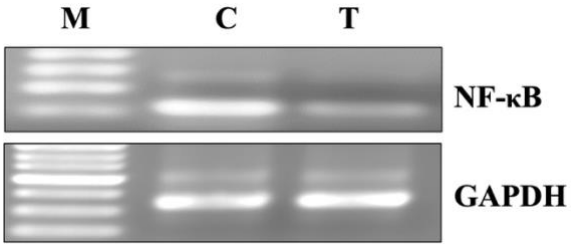


Figure 3. Inactivation of *NF-kB* gene expression in EAC cells treated with RTNSME. UV-trans illuminator visualizations of *NF-kB* and GAPDH. Here, M: Marker, C: Untreated EAC cells, and T: EAC cells treated with RTNSME.

Intracellular ROS in EAC cells

A fluorescent probe, DCFH-DA, is used for sensing ROS in cells. As shown in Figure 4, both the untreated control and RTNSME-treated EAC cells displayed a similar pattern of green fluorescence in ROS-positive cells. No significant difference is found between the two.

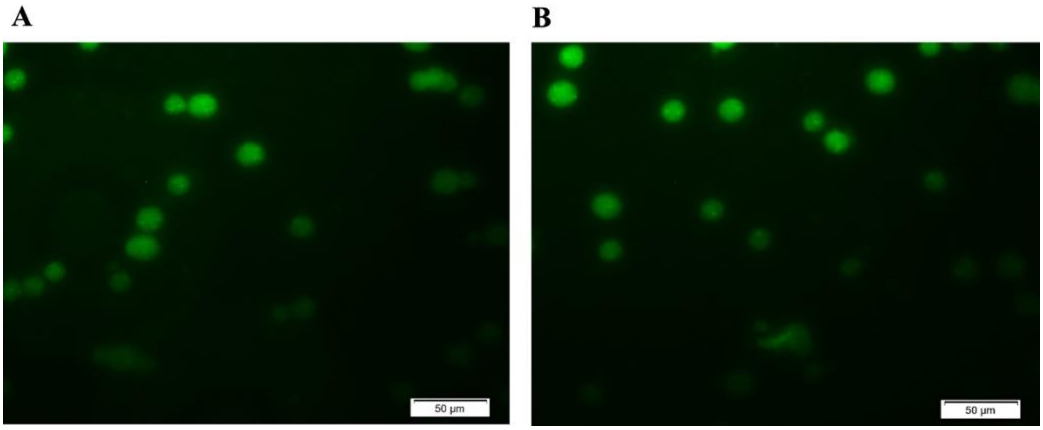


Figure 4. Intracellular ROS generation in EAC cells. Visualization of cells under a fluorescence microscope after incubation with DCFH-DA. A) Untreated EAC cells, and B) EAC cells treated with RTNSME.

Chemical composition of RTNSME

GC/MS chromatogram (Figure 5) and list of compounds (Table 2) revealed that RTNSME consists of 35 compounds of different chemical families. Literature review revealed that cell growth inhibitory activity has been found in canthaxanthin [27-32], colchiceinamide derivatives [33,34], and dipyridamole [35] among the 35 compounds.

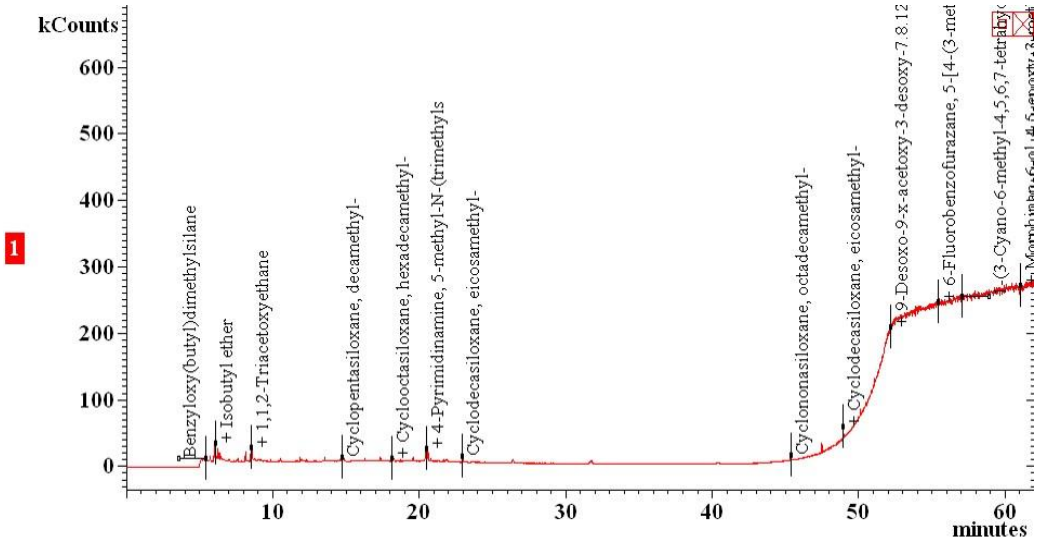


Figure 5. GC/MS chromatogram of RTNSME.

Table 2. Chemical composition of RTNSME analyzed by GC/MS.

SL	Compound Name	MW	Formula	RT	Area %
1	Benzyloxy(butyl)dimethylsilane	222	$C_{13}H_{22}OSi$	5.46	1.4
2	Isobutyl ether	130	$C_8H_{18}O$	6.06	6.16
3	1-(Nitromethyl)-cyclohexanol	159	$C_7H_{13}NO_3$	5.26	2.26
4	Ethanol, 2-butoxy-	118	$C_6H_{14}O_2$	6.39	2.50
5	1,2,3-Propanetriol, monoacetate	134	$C_5H_{10}O_4$	8.14	1.65
6	Benzyl Alcohol	108	C_7H_8O	8.48	1.50
7	1,1,2-Triacetoxyethane	204	$C_8H_{12}O_6$	8.57	3.81
8	Cyclopentasiloxane, decamethyl-	370	$C_{10}H_{30}O_5Si_5$	14.77	0.43
9	Cyclohexasiloxane, dodecamethyl-	444	$C_{12}H_{36}O_6Si_6$	17.33	0.95

10	Cyclooctasiloxane, hexadecamethyl-	592	$C_{16}H_{48}O_8Si_8$	18.13	3.44
11	Cycloheptasiloxane, tetradecamethyl-	518	$C_{14}H_{42}O_7Si_7$	19.59	0.82
12	4-Pyrimidinamine, 5-methyl-N-(trimethylsilyl)-2-[(trimethylsilyl)oxy]-	269	$C_{11}H_{23}N_3OSi_2$	20.47	5.04
13	Octadecamethyl-Cyclononasiloxane	666	$C_{18}H_{54}O_9Si_9$	20.60	6.53
14	Cyclodecasiloxane, eicosamethyl-	740	$C_{20}H_{60}O_{10}Si_{10}$	22.95	4.03
15	gamma.-Lumicolchicine	399	$C_{22}H_{25}NO_6$	49.71	2.07
15	3,9.beta.;14,15-Diepoxypregn-16-en-20-one, 3,11.beta.,18-triacetoxy-	502	$C_{27}H_{34}O_9$	50.05	4.03
16	2-Butenoic acid, 2-methyl-, 1,1a,1b,4,4a,5,7a,7b,8,9-decahydro-4a,7b-dihydroxy-3-(hydroxymethyl)-1,1,6,8-tetramethyl-5-oxo-9aH-cyclopropa[3,4]benz[1,2-e]azulene-9,9a-diyl ester, [1aR-[1a.alpha.,1b.beta.,4a.beta.,7a.alpha.,7b.alpha.,8.alpha.,9.beta.(E),9a.alpha.(E)]]-	528	$C_{30}H_{40}O_8$	50.35	1.00
17	psi.,.psi.-Carotene, 3,4-didehydro-1,2,7',8'-tetrahydro-1-methoxy-2-oxo-	582	$C_{41}H_{58}O_2$	50.52	4.17
18	9-Desoxo-9-x-acetoxy-3,8,12-tri-O-acetylingol	536	$C_{28}H_{40}O_{10}$	51.52	2.6
19	Canthaxanthin	564	$C_{40}H_{52}O_2$	51.67	5.38
20	Colchiceinamide	384	$C_{21}H_{24}N_2O_5$	51.76	2.67
21	Norcodeine di-TMS derivative	429	$C_{23}H_{35}NO_3Si_2$	51.86	3.64
22	2,4-Imidazolidinedione, 5-[3,4-bis[(trimethylsilyl)oxy]phenyl]-3-methyl-5-phenyl-1-(trimethylsilyl)	516	$C_{25}H_{40}N_2O_4Si_3$	51.90	2.09
23	3,8,12-Triacetylingol 7-(4-methoxyphenyl)acetate	640	$C_{35}H_{44}O_{11}$	51.97	1.52
24	6,6'-Diacetyl-7,7'-dihydroxy-2,2',4,4',5,5'-hexamethoxy-1,1'-binaphthalene	550	$C_{30}H_{30}O_{10}$	52.08	3.95
25	D-Glucopyranosiduronic acid, 3-(5-ethylhexahydro-1,3-dimethyl-2,4,6-trioxo-5-pyrimidinyl)-1-methylbutyl 2,3,4-tris-O-(trimethylsilyl)-, methyl ester	676	$C_{29}H_{56}N_2O_{10}Si_3$	52.26	3.72
26	Pregnane-11,20-dione, 3,17,21-tris[(trimethylsilyl)oxy]-, 20-[O-(phenylmethyl)oxime], (3.alpha.,5.alpha.)-	685	$C_{37}H_{63}NO_5Si_3$	52.35	2.24
27	Cephalotaxine, 11-(acetyloxy)-, acetate (ester), (11.alpha.)-	415	$C_{22}H_{25}NO_7$	52.41	1.97
28	Silane, [[(3.beta.,5.alpha.,11.beta.,20S)-pregnane-3,11,17,20,21-pentayl]pentakis(oxy)]pentakis[trimethyl-	728	$C_{36}H_{76}O_5Si_5$	52.52	1.90
29	5H-Cyclopropa[3,4]benz[1,2-e]azulen-5-one, 2,4a,9,9a-tetrakis(acetyloxy)-3,[(acetyloxy)methyl]-1,1a,1b,2,3,4,4a,7a,7b,8,9,9a-dodecahydro-2,7b-dihydroxy-1,1,6,8-tetramethyl-, [1aR-(1a.alpha.,1b.beta.,2.alpha.,3.beta.,4a.beta.,7a.alpha.,7b.alpha.,8.alpha.,9.beta.,9a.alpha.)]-	608	$C_{30}H_{40}O_{13}$	52.70	0.77
30	Dipyridamole	504	$C_{24}H_{40}N_8O_4$	52.82	0.70
31	6-Fluorobenzofurazane, 5-[4-(3-methoxyphenyl)piperazin-1-yl]-, 1-oxide	344	$C_{17}H_{17}FN_4O_3$	55.45	0.86
32	1-(3-Cyano-6-methyl-4,5,6,7-tetrahydro-thieno[2,3-c]pyridin-2-yl)-3-phenyl-thiourea	328	$C_{16}H_{16}N_4S_2$	57.04	0.35
33	Morphinan-6-ol, 4,5-epoxy-3-methoxy-17-methyl-, acetate (ester), (5.alpha.,6.alpha.)-	343	$C_{20}H_{25}NO_4$	61.02	1.35
34	Echinenone	550	$C_{40}H_{54}O$	61.50	0.43
35	2,2'-Binaphthalene]-8,8'-dicarbonitrile, 1,1'-dihydroxy-6,6',7,7'-tetramethoxy-3,3'-dimethyl-5,5'-bis(1-methylethyl)-	568	$C_{34}H_{36}N_2O_6$	61.87	0.80

Molecular docking simulation

Among the three compounds, no significant binding of Dipyridamole with Bax, Bcl-2, p53, and NF-kB was observed, as shown in Table 3. Although a significant binding of Colchiceinamide was found only with Bcl-2, with the binding energy of -7.5 kcal/mol (Figure 6A). Where Colchiceinamide formed two hydrogen bonds with residues ASN180 and SER81. Besides the hydrogen bonds, other types of bonding were also observed (Figure 6A). But Canthaxanthin exerts strong binding affinity with Bax, Bcl-2, p53, and NF-kB proteins with the binding energy of -7.8, -8.6, -7.0, and -7.0 kcal/mol, respectively (Table 3). No hydrogen bonding was observed for Bax and Bcl-2 (Figures 6B and C). But strong hydrogen bonding was observed for NF-kB (Figure 6D) and p53 (Figure 6E). Besides hydrogen bonding, other types of interactions were also observed for each of the proteins, as shown in the 2D picture (Figure 6).

Table 3. Binding energy.

Protein Name	Compound Name	Binding energy (kcal/mol)
Bax	Canthaxanthin	-7.8
Bax	Colchiceinamide	-6.0
Bax	Dipyridamole	-5.4
Bcl-2	Canthaxanthin	-8.6
Bcl-2	Colchiceinamide	-7.5
Bcl-2	Dipyridamole	-6.0
p53	Canthaxanthin	-7.0
p53	Colchiceinamide	-5.9
p53	Dipyridamole	-5.4
NF-kB	Canthaxanthin	-7.0
NF-kB	Colchiceinamide	-5.6
NF-kB	Dipyridamole	-5.4

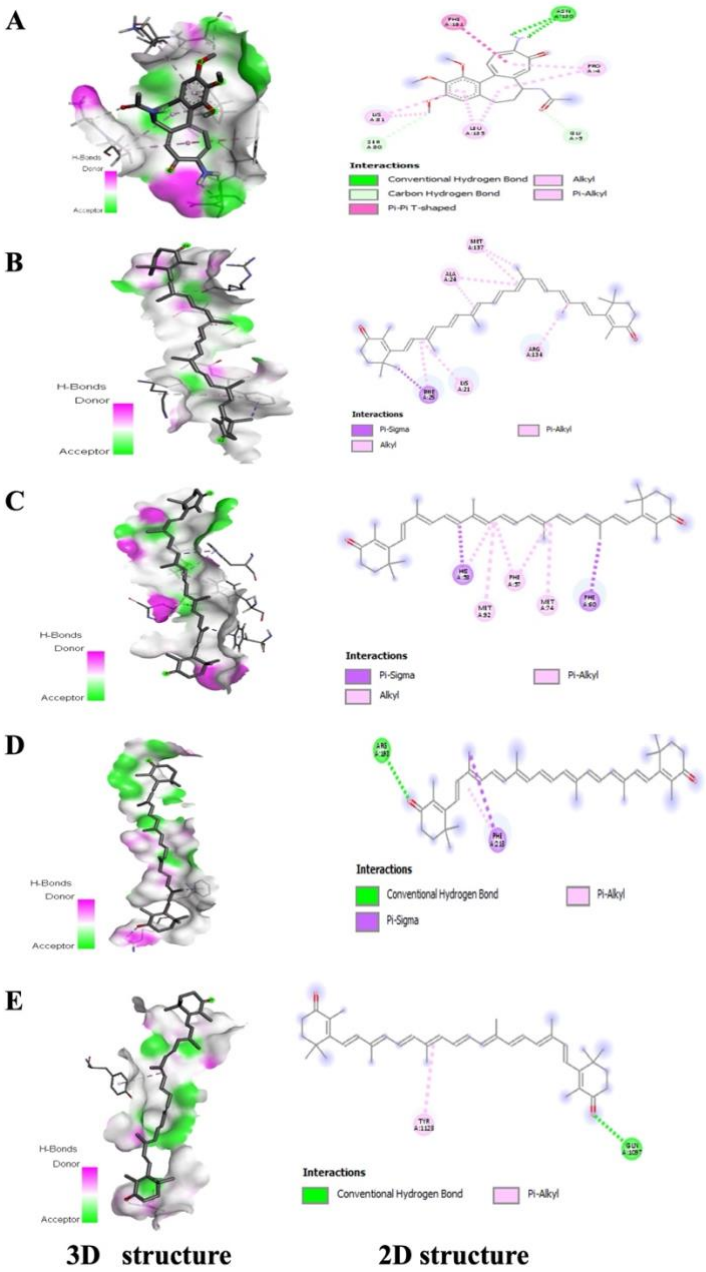


Figure 6. Binding affinity between Dipyridamole, Colchiceinamide, and Canthaxanthin with different proteins. A) Represents binding of Colchiceinamide with Bcl-2. While B-E) indicates the interaction between Canthaxanthin and Bax, Bcl-2, p53, and NF-kB, respectively.

DISCUSSION

The primary objective of this study was to evaluate the growth-inhibitory effects of RTNSME in EAC cells. The findings of this study provide clear evidence that RTNSME possesses significant growth inhibitory activity, primarily by inducing apoptosis.

Due to the lack of apoptosis, cancer cells continue to grow, which causes the severity of cancer [36]. In Figure 1, our results demonstrated that RTNSME exhibited a dose-dependent growth inhibitory effect in EAC cells. Furthermore, DAPI staining of untreated EAC cells and of RTNSME-treated cells revealed some morphological alterations, including membrane blebbing, cell shrinkage, and nuclear condensation (Figure 2A), which are indicative features of apoptotic cell death. Therefore, these results suggest that RTNSME effectively inhibits cell growth by triggering apoptotic processes.

p53, Bax, Bcl-2, and caspase 3 are some proteins that regulate cell apoptosis. [37]. Molecular studies revealed that p53 up-regulation, Bcl-2 down-regulation, and Bax up-regulation indicate mitochondrial dysfunctional apoptosis [38]. In this study, the expression of *p53*, *Bax,* and *Bcl-2* mRNA was investigated. Upregulation of *p53* and *Bax,* and down-regulation of *Bcl-2* were found in RTNSME-treated EAC cells compared to untreated cells, as shown in Figure 2B. This result indicates mitochondrial dysfunction-mediated apoptosis. Taken together, morphological changes in untreated EAC cells and reciprocal expression of pro-apoptotic and anti-apoptotic genes support RTNSME-treated EAC cell growth inhibition.

NF-kB is a key regulator involved in cell growth, survival, and apoptosis induction [22,39]. In cancer, NF-kB is typically up-regulated, promoting inflammation and facilitating tumorigenesis [40], while also driving metastasis [23]. Activation of NF-kB generally inhibits p53 function [24,25], meaning that p53 and NF-kB often exhibit opposing effects in cancer cells [26]. In this study, we found that RTNSME inhibited NF-kB activation (Figure 3) in conjunction with growth inhibition, suggesting that NF-kB inactivation could initiate apoptotic pathways and contribute to EAC cell death.

Some reports showed decreased NF-kB activity with increased ROS [17,18,41]. Since inhibition of the transcription factor NF-kB leads to increased accumulation of ROS. NF-kB has been reported to suppress antioxidant gene expression [42-44]. Numerous compounds confirmed cell death in cancer cells with NF-κB inactivation and elevated ROS levels [17, 18]. In this study, reduced NF-kB activity was observed, but no significant changes in ROS in RTNSME-treated EAC cell death. Here, no reciprocal relation was found. To clarify this issue, further studies are needed.

GC-MS analysis of RTNSME identified 35 compounds, many of which are known to possess biological activity. Notably, Canthaxanthin, a compound found in RTNSME, has been reported to act as an anti-tumor agent [27-32]. Previous studies have demonstrated that Canthaxanthin inhibits the growth of murine melanoma, fibrosarcoma, and human squamous carcinoma cells in vitro [31] and can reduce cell growth by inducing apoptosis [32]. Dipyridamole, also present in RTNSME, has shown antitumor activity and can enhance the sensitivity of several chemotherapy agents, including 5-fluorouracil, cisplatin, and methotrexate [34]. Additionally, Colchiceinamide found in RTNSME has demonstrated anticancer potential across various cancer cell lines [35]. Consequently, the synergistic activity of these compounds in RTNSME might be the possible reason.

Molecular docking, a critical tool in computational drug design, was employed in this study to investigate the interaction between RTNSME compounds and key apoptosis-

regulating proteins (Bax, Bcl-2, p53, and NF-kB). Our docking results revealed a strong binding affinity between canthaxanthin and these proteins, supporting the activation of apoptotic pathways via the modulation of these key regulatory proteins.

CONCLUSIONS

RTNSME significantly inhibited EAC cell growth by inducing apoptosis. This growth inhibitory effect is likely mediated through mitochondrial dysfunction, with reciprocal changes in the expression level of *Bax* and *Bcl-2*. Furthermore, inactivation of *NF-kB* and up-regulation of *p53* appear to play central roles in promoting EAC cell death. Our findings suggest that RTNSME down-regulates *NF-kB*, which in turn up-regulates *p53*, leading to apoptosis in EAC cells (Figure 7).

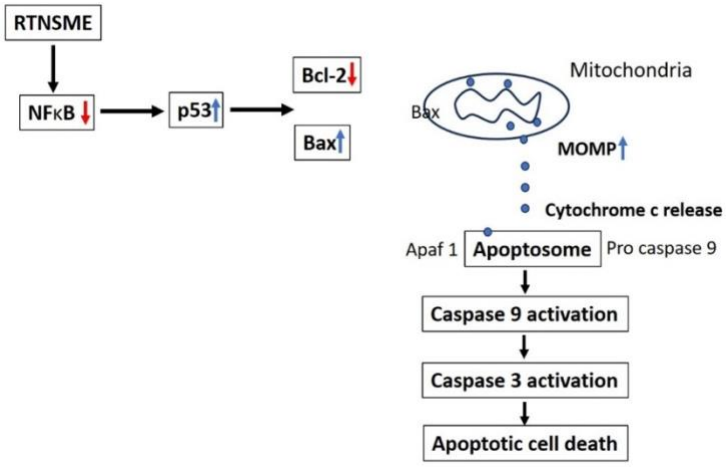


Figure 7. Proposed hypothetical schematic diagram of growth inhibition of EAC cells through apoptosis in relation to *NF-kB* inactivation treated with RTNSME. RTNSME might up-regulate *p53* gene expression and allow subsequent signalling for cell death through apoptosis, as discussed in this report.

ACKNOWLEDGEMENTS

None.

AUTHOR CONTRIBUTIONS

SYA and MAS designed the study, performed the experiment, and drafted the manuscript. MI and MH analyzed the data and generated figures and tables. SRK supported docking experiments; FI edited the manuscript. MAR planned, supervised the project, and edited the manuscript.

CONFLICTS OF INTEREST

There is no conflict of interest among the authors.

DATA AVAILABILITY

This manuscript was uploaded to Research Square as a preprint: https://doi.org/10.21203/rs.3.rs-6950088/v1.

REFERENCES

[1] Abdullaev FI, Rivera-Luna R, et al. Pattern of childhood cancer mortality in Mexico. Arch Med Res. 2000;31(5):526-531.

[2] Islam F, Gopalan V, et al. Kaempferia rotunda tuberous rhizome lectin induces apoptosis and growth inhibition of colon cancer cells in vitro. Int J Biol Macromol. 2019; 141:775-782.

[3] Das PK, Rakib MA, et al. Novel Therapeutics Against Breast Cancer Stem Cells by Targeting Surface Markers and Signaling Pathways. Curr Stem Cell Res Ther. 2019;14(8):669-682.

[4] Khatun M, Habib MR, et al. Antioxidant, cytotoxic and antineoplastic effects of Carissa carandas Linn. leaves. Exp Toxicol Pathol. 2017;69(7):469-476.

[5] Islam F, Khatun H, et al. Growth inhibition and apoptosis of Ehrlich ascites carcinoma cells by the methanol extract of Eucalyptus camaldulensis. Pharm Biol. 2014;52(3):281-290.

[6] Institute of Botany, the Chinese Academy of Sciences, 2004. Iconographia Cormophytorum Sinicorum (Tomus). Science Press, Beijing, China, 52,167.

[7] Faruk MO, Amin MZ, et al. Biochemical analysis of two varieties of water chestnuts (Trapa sp.). Pak J Biol Sci. 2012;15(21):1019-1026.

[8] Parekh J, Chanda S. In vitro antimicrobial activity of Trapa natans L. fruit rind extracted in different solvents. Afr. J. Biotechnol. 2007;6(6): 766-770.

[9] Anjani S, Ranjeet SK, et al. Evaluation of analgesic activity of methanolic root extracts of Trapa bispinosa roxb. International Journal of Pharmacology and Clinical Research 2025; 7(1): 10-15.

[10] Patel S, Banji D, et al. Scrutinizing the role of aqueous extract of Trapa bispinosa as an immunomodulator in experimental animals. Int. J. Res. Pharm. Sci. 2010: 1(1): 13-19.

[11] Huang HC, Chao CL, et al. Hypoglycemic Constituents Isolated from Trapa natans L. Pericarps. J Agric Food Chem. 2016;64(19):3794-3803.

[12] Chandana M, Mazumder R, et al. A review on potential of plants under Trapa species. Int. j. res. pharm. pharm. sci. 2013;3(2):502-8.

[13] Gani A, Rasool N, et al. DNA scission inhibition, antioxidant, and antiproliferative activities of water chestnut (*Trapa natans*) extracted in different solvents. *CyTA* - Journal of Food 2015;*13*(3):415–419.

[14] Asha SH, Siddika A, et al. Phytochemical profiling and antioxidant activity of different varieties of Trapa natans: A comparative analysis. J Pharmacogn Phytochem 2024; 13(5): 232-237.

[15] Olayaki LA, Irekpita JE, et al. Methanolic extract of Moringa oleifera leaves improves glucose tolerance, glycogen synthesis and lipid metabolism in alloxan-induced diabetic rats. J Basic Clin Physiol Pharmacol. 2015;26(6):585-593.

[16] Syed Abdul Rahman SN, Abdul Wahab N, et al. In Vitro Morphological Assessment of Apoptosis Induced by Antiproliferative Constituents from the Rhizomes of Curcuma zedoaria. Evid Based Complement Alternat Med. 2013; 2013:257108.

[17] Das PK, Asha SY, et al. Methanolic extract of Moringa oleifera leaves mediates anticancer activities through inhibiting NF-*κ*B and enhancing ROS in Ehrlich ascites carcinoma cells in mice. J Adv Biotechnol Exp Ther. 2021; 4(2): 161-170.

[18] Rakib MA, Lee WS, et al. Antiproliferative Action of Conjugated Linoleic Acid on Human MCF-7 Breast Cancer Cells Mediated by Enhancement of Gap Junctional Intercellular Communication through Inactivation of NF- κ B. Evid Based Complement Alternat Med. 2013;2013:429393.

[19] Chen J. The Cell-Cycle Arrest and Apoptotic Functions of p53 in Tumor Initiation and Progression. Cold Spring Harb Perspect Med. 2016;6(3): a026104.

[20] Pellegata NS, Antoniono RJ, et al. DNA damage and p53-mediated cell cycle arrest: a reevaluation. Proc Natl Acad Sci U S A. 1996;93(26):15209-15214.

[21] Meyer C, Sims AH, et al. Transcript and protein profiling identifies signaling, growth arrest, apoptosis, and NF-κB survival signatures following GNRH receptor activation. Endocr Relat Cancer. 2013;20(1):123-136.

[22] Xia Y, Shen S, et al. NF-κB, an active player in human cancers. Cancer Immunol Res. 2014;2(9):823-830.

[23] Dey A, Tergaonkar V, et al. Double-edged swords as cancer therapeutics: simultaneously targeting p53 and NF-kappaB pathways. Nat Rev Drug Discov. 2008;7(12):1031-1040.

[24] Ak P, Levine AJ. p53 and NF-κB: different strategies for responding to stress lead to a functional antagonism. FASEB J. 2010;24(10):3643-3652.

[25] Carrà G, Lingua MF, et al. P53 vs NF-κB: the role of nuclear factor-kappa B in the regulation of p53 activity and vice versa. Cell Mol Life Sci. 2020;77(22):4449-4458.

[26] Sadati S, Khalaji A, et al. NF-κB and apoptosis: colorectal cancer progression and novel strategies for treatment. Eur J Med Res. 2025;30(1):616.

[27] Tanaka T, Makita H, et al. Chemoprevention of rat oral carcinogenesis by naturally occurring xanthophylls, astaxanthin and canthaxanthin. Cancer Res. 1995;55(18):4059-4064.

[28] Tanaka T, Kawamori T, et al. Suppression of azoxymethane-induced rat colon carcinogenesis by dietary administration of naturally occurring xanthophylls astaxanthin and canthaxanthin during the postinitiation phase. Carcinogenesis. 1995;16(12):2957-2963.

[29] Grubbs CJ, Eto I, et al. Effect of canthaxanthin on chemically induced mammary carcinogenesis. *Oncology*. 1991;48(3):239-245.

[30] Katsumura N, Okuno M, et al. Suppression of mouse skin papilloma by canthaxanthin and beta-carotene in vivo: possibility of the regression of tumorigenesis by carotenoids without conversion to retinoic acid. Nutr Cancer 1996;26(2):203-208.
[31] Huang DS, Odeleye OE, et al. Inhibitory effects of canthaxanthin on in vitro growth of murine tumor cells. Cancer Lett. 1992;65(3):209-213.
[32] Palozza P, Maggiano N, et al. Canthaxanthin induces apoptosis in human cancer cell lines. Carcinogenesis 1998;19(2):373-376.
[33] Li-Hong S, Hong-Yu Li, et al. Synthesis and cytotoxic evaluation of new colchicine derivatives bearing 1,3,4-thiadiazole moieties, Chin. Chem. Lett. 2013;24(4):299-302.
[34] Kumar A, Sharma PR, et al. Potential anticancer role of colchicine-based derivatives: an overview. Anticancer Drugs. 2017;28(3):250-262.
[35] Ge SM, Zhan DL, et al. Reverse screening approach to identify potential anti-cancer targets of dipyridamole. Am J Transl Res. 2016;8(12):5187-5198.
[36] Elmore S. Apoptosis: a review of programmed cell death. Toxicol Pathol. 2007;35(4):495-516.
[37] Tsujimoto Y. Role of Bcl-2 family proteins in apoptosis: apoptosomes or mitochondria? Genes Cells. 1998;3(11):697-707.
[38] Naseri MH, Mahdavi M, et al. Up regulation of Bax and down regulation of Bcl2 during 3-NC mediated apoptosis in human cancer cells. Cancer Cell Int. 2015; 15:55.
[39] Alonso F, Krattinger N, et al. An angiotensin II- and NF-kappaB-dependent mechanism increases connexin 43 in murine arteries targeted by renin-dependent hypertension. Cardiovasc Res. 2010;87(1):166-176.
[40] Baud V, Karin M. Is NF-kappaB a good target for cancer therapy? Hopes and pitfalls. Nat Rev Drug Discov. 2009;8(1):33-40.
[41] Jin Y, Lu Z, et al. Antineoplastic mechanisms of niclosamide in acute myelogenous leukemia stem cells: inactivation of the NF-kappaB pathway and generation of reactive oxygen species. Cancer Res 2010; 70:2516-27.
[42] Lampiasi N, Azzolina A, D'Alessandro N, Umezawa K, McCubrey JA, Montalto G, et al. Antitumor effects of dihydroxymethylepoxyquinomicin, a novel nuclear factor kappaB inhibitor, in human liver cancer cells are mediated through a reactive oxygen species-dependent mechanism. Mol Pharmacol 2009; 76:290-300.
[43] Stein SJ, Baldwin AS. NF-κB suppresses ROS levels in BCRABL (+) cells to prevent activation of JNK and cell death. Oncogene 2011; 30:4557-66.
[44] Pozo-Guisado E, Merino JM, et al. Resveratrol-induced apoptosis in MCF-7 human breast cancer cells involves a caspase-independent mechanism with downregulation of Bcl-2 and NF-kappaB. Int J Cancer 2005; 115:74-84.

Disclaimer: The contents of all publications are solely those of the individual author(s) and contributor(s) and not of JABET and/or the editor(s). JABET and/or the editor(s) disclaim responsibility for any injury to people or property resulting from any of the contents.